J Solid State Electrochem (2007) 11:1157–1162
DOI 10.1007/s10008-006-0255-3

ORIGINAL PAPER

Studies on structure and electrochemical properties of pillared M–MnO_2 (M=Ba^{2+}, Sr^{2+}, ZrO^{2+})

Yanluo Lu · Lan Yang · Min Wei · Yaning Xie · Tao Liu

Received: 4 September 2006 / Revised: 27 November 2006 / Accepted: 8 December 2006 / Published online: 5 January 2007

Abstract Supramolecular pillared oxides $M-MnO_2$ $\left(M = Ba^{2+}, Sr^{2+}, ZrO^{2+}\right)$ were prepared through the intercalation of M^{2+} cations into a MnO_2 host matrix by the method of ion exchange between the precursor δ-K_xMnO_2 and the corresponding guest. The materials M-MnO_2 crystallize in the hexagonal system, the same structure as the precursor, with a larger interlamellar spacing. In the case of ZrO-MnO_2, extended X-ray absorption fine structure (EXAFS) determination indicates that the Zr atom locates between the MnO_2 layers forming a stable structure. Compared with the precursor, the cycling property of M-MnO_2 was improved distinctly, while the capacity decreased to some degree due to the strong interaction between pillars and the host matrix. Among these pillared materials, ZrO-MnO_2 has an advanced reversible capacity of 161.5 $mAh{\cdot}g^{-1}$ and improved cycling behavior compared with the precursor.

Keywords Layered M-MnO_2 · Cathode materials · Lithium secondary batteries · Intercalation · Electrochemical properties

Y. Lu · L. Yang · M. Wei (✉)
State Key Laboratory of Chemical Resource Engineering,
Beijing University of Chemical Technology,
Beijing 100029, People's Republic of China
e-mail: weimin@mail.buct.edu.cn

Y. Xie · T. Liu
Beijing Synchrotron Radiation Facility,
Institute of High Energy Physics, Chinese Academy of Sciences,
Beijing 100049, People's Republic of China

Introduction

Cathode materials for rechargeable lithium ion batteries have been the focus of intensive research for a number of years. Among the candidates for cathodic materials, manganese oxides are particularly attractive due to the low cost of raw materials and the fact that manganese is considered more environmentally friendly than other transition metals, such as cobalt and nickel. Considerable interest is currently focused on layered $LiMnO_2$, because a layered structure allows ready intercalation and deintercalation of lithium ions.

Due to the Jahn-Teller distortions of Mn^{3+} ions, the structure of layered $LiMnO_2$ has been demonstrated to be unstable [1–3] and it transforms to spinel easily. Being cathode materials for lithium ion batteries, the charge-discharge capacity of layered $LiMnO_2$ decreases quickly and the materials have a short cycling life. Doping $LiMnO_2$ by replacing part of the Mn with transition metal elements such as Co, Ni and Cr has been carried out [4, 5], and it was reported that both the structural stability and electrochemical performance (including capacity and retention) of layered $LiMnO_2$ can be improved by doping. However, these compounds were found to convert to a spinel phase during cycling.

Pillaring the layered materials is another feasible method to enhance the charge-discharge stability [6, 7], for the interlamellar space can be expanded by large ions. Whittingham et al. [6] reported the synthesis of layered potassium manganese oxide with interlayer spacing of 7.0 Å by mild hydrothermal decomposition of the permanganate salt, and they found that the structural stability and electrochemical properties were improved owing to small amounts of potassium ions and H_2O molecules between the MnO_2 sheets acting as pillars. F. Zhang et al. [7] reported

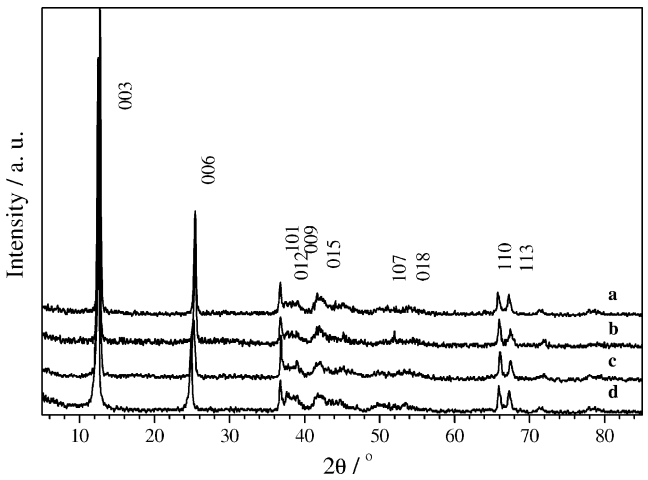

Fig. 1 XRD patterns for the precursor and the products $M-MnO_2(M=Ba^{2+},Sr^{2+},ZrO^{2+})$ **a** Precursor K_xMnO_2. **b** Ba-MnO_2. **c** Sr-MnO_2. **d** ZrO-MnO_2

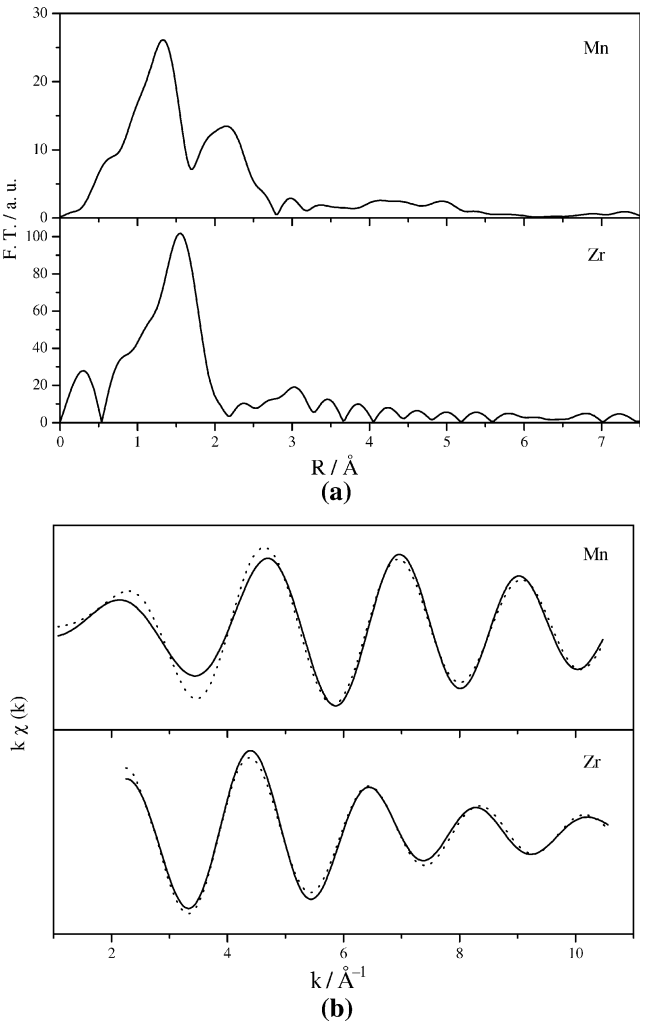

Fig. 2 **a** Fourier transforms of Mn and Zr K-edges EXAFS of ZrO-MnO_2. **b** k-space data for Mn and Zr (*solid curve* experiment; *dashed curve* fitted curve)

that the interlayer spacing of MnO_2 pillared by VO^{2+} reaches 7.36 Å. Furthermore, the organic-inorganic composite materials based on pillared vanadium oxides [8–14], such as $K_{0.16}Mn_{0.04}V_2O_{4.94}\cdot 0.14H_2O$ [14] and δ-$[N(CH_3)_4]_zMn_yV_2O_5\cdot nH_2O$ [13], were obtained through the reaction between vanadium oxide and metal ions (or tetramethyl ammonium).

In this paper, supramolecular pillared oxides $M-MnO_2(M=Ba^{2+},Sr^{2+},ZrO^{2+})$ were prepared by intercalating the guest cations into a MnO_2 host matrix. The structure and composition of the products have been characterized by X-ray diffraction (XRD), extended X-ray absorption fine structure (EXAFS) and inductively coupled plasma emission (ICP). Moreover, their performance as cathode material in lithium secondary batteries has been examined.

Experimental

Preparation of the precursor δ-K_xMnO_2: δ-K_xMnO_2 was obtained by thermal decomposition of $KMnO_4$ [15]. Potassium permanganate powder was calcined at 600 °C in air for 5 h, then washed thoroughly with distilled water and dried at 70 °C for 12 h, and thus layered δ-K_xMnO_2 was obtained.

Table 1 Lattice parameters of the precursor and the products M-MnO_2

	d_{003}/nm	d_{110}/nm	a/nm	c/nm	c/a
K_xMnO_2	0.6955	0.1418	0.2836	2.0865	7.357
Ba-MnO_2	0.6976	0.1415	0.2830	2.0928	7.395
Sr-MnO_2	0.7006	0.1414	0.2828	2.1018	7.432
ZrO-MnO_2	0.7111	0.1417	0.2834	2.1333	7.528

Preparation of $M-MnO_2(M=Ba^{2+},Sr^{2+},ZrO^{2+})$: δ-$K_xMnO_2$ was firstly mixed with 1 M aqueous HCl solution with vigorous agitation for 10 h at room temperature and subsequently washed with distilled water. The product was then added into a solution of $Ba(NO_3)_2$, $Sr(NO_3)_2$ and $ZrOCl_2$ respectively, and agitated for 24 h at room temperature to obtain $M-MnO_2(M=Ba^{2+},$

Table 2 EXAFS results for ZrO-MnO_2

	N	R/Å	σ^2/Å^2	R_f/%
Mn-O	5.2	1.85	0.005	19.4
Zr-O	6.1	2.12	0.005	11.0

N coordination number, R interatomic distance, σ Debye-Waller factor, R_f a measure of the agreement between experimental and theoretical EXAFS curves. R_f <20% indicates a very good fit. The precision of N is estimated to be ≤20%.

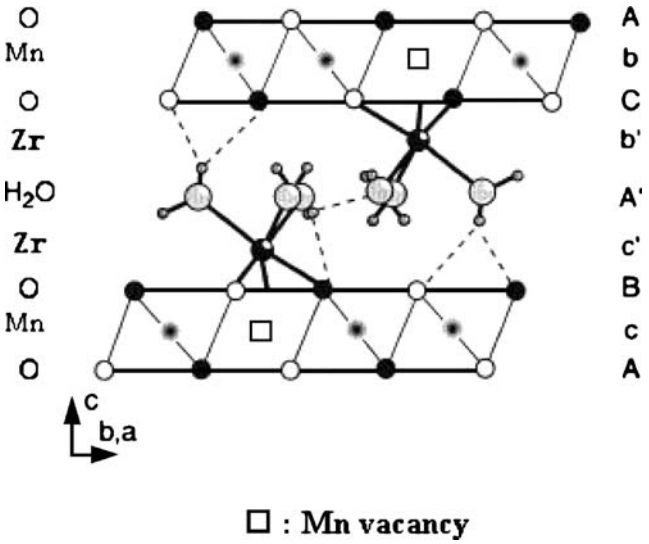

Fig. 3 Schematic structure of the pillared material ZrO-MnO_2

Sr^{2+}, ZrO^{2+}). All of the samples were dried at 70 °C for 12 h in air before characterization.

XRD patterns were recorded using a Shimadzu XRD-6000 diffractometer in the range $5 \leq 2\theta \leq 85°$ using a monochromatized Cu Kα radiation source ($\lambda = 0.154$ nm). EXAFS data were collected at the Beijing Synchrotron Radiation Facility and analyzed with the Crius2 XAFS program (Daresbary). Raw spectra were Fourier transformed to *R* space. The atomic distance *R* and the coordination number *N* of the sample were calculated by performing curve fitting with nonlinear least-squares. Elemental analysis was performed by ICP spectroscopy using a Shimadzu ICPS-7500 instrument. The average oxidation state of Mn was determined by chemical redox titration.

In order to evaluate the electrochemical performance of the material, composite electrodes were formed by mixing the active material with acetylene black and polytetrafuoroethylene (PTFE) in the weight ratio 85/10/5, and then pressing into pellets. PTFE was pre-dispersed in the mixture of water and ethanol before mixing with the other components. The active material and acetylene black were mixed sufficiently by grinding together, then added into dispersant. After the solvent was evaporated at 120 °C in air, the components were pressed. The pellets were cut (diameter: 5 mm; thickness: 80–100 μm; quality: 10–12 mg) and dried at 120 °C in vacuum for 24 h before use. Button-type cells were assembled in a glove box filled with argon with less than 1 ppm H_2O and O_2. The case of the coin battery made by stainless steel consisted of a lid serving as the cathode, a lid serving as the anode, and a PTFE gasket to insulate the cathode from the anode. At first one lid was screwed to the PTFE case, then stainless steel plate, the anode, separator, the cathode and stainless steel plate were placed in the case in turn; later, about 0.5 ml electrolyte was infused and finally the battery case was covered with the lid and screwed firmly in place. The anode was metallic lithium disk (diameter: 6 mm; thickness: 600 μm) and the electrolyte was 1 M $LiClO_4$ dissolved in a mixture of ethylene carbonate (EC) and diethylene carbonate (DEC) in the volume ratio 1/1. The galvanostatic charge-discharge tests were carried out between 2.0–4.0 V (versus Li/Li^+) at a constant current density of 0.2 $mA \cdot cm^{-2}$ (corresponding to the 0.07C rate) using a LAND CT2001A cycle life tester.

Results and discussion

Structure and composition of the manganese oxides

It is known that $KMnO_4$ decomposes into a mixture of potassium manganate(VI), manganate(V) and MnO_2 upon heating above 200 °C in air [15]. The decomposition reaction can be expressed simply as follows:

$$5KMnO_4 \rightarrow K_2MnO_4 + K_3MnO_4 + 3MnO_2 + 3O_2 \uparrow$$

After washing with distilled water, soluble products such as K_2MnO_4 and K_3MnO_4 can be removed, and thus δ-K_xMnO_2 powder is obtained. The powder XRD pattern of the resulting δ-K_xMnO_2 is shown in Fig. 1. The reflection can be indexed using the standard pattern on a simple three-block cell, commonly used for the description of layered manganese oxide [16]. The calculated lattice parameters of the sample are: $a = 0.2837$ nm and $c = 2.0865$ nm, with a corresponding repeat distance of 0.696 nm. The *c* value in this work is larger than that of the literature ($a = 0.2880$ nm, $c = 1.900$ nm [16] for hexagonal $K_{0.47}Mn_{0.94}O_2$), owing to some H_2O existing in the interlamellar space and different K content. Elemental analysis of δ-K_xMnO_2 confirms that the value of *x* is 0.30, less than the reported data. Chen et

Table 3 Mean oxidation state of Mn and chemical compositions of the precursor and the pillared products

	Mn wt.%	K wt.%	M wt.% $(M = Ba^{2+}, Sr^{2+}, Zr^{4+})$	Mean valence of Mn	Composition
K_xMnO_2	51.94	11.26	–	3.86	$K_{0.30}MnO_{2.08} \cdot 0.31H_2O$
Ba-MnO_2	47.16	0.21	15.29	3.79	$Ba_{0.13}K_{0.006}MnO_{2.03} \cdot 0.61H_2O$
Sr-MnO_2	52.49	2.33	6.34	3.80	$Sr_{0.076}K_{0.062}MnO_{2.01} \cdot 0.47H_2O$
ZrO-MnO_2	52.67	1.87	6.99	3.79	$(ZrO)_{0.08}K_{0.05}MnO_{2.00} \cdot 0.38H_2O$

al. [6] have reported that layered $K_xMnO_2{\cdot}yH_2O$ can be synthesized by reaction of potassium permanganate with hydrochloric acid followed by hydrothermal treatment of the mixture. The XRD pattern of δ-K_xMnO_2 in this work (Fig. 1) is similar to that of Chen's work, in which the lattice repeat distance was around 0.70 nm.

Pillared M-MnO_2 materials were obtained by the method of ion-exchange. Figure 1 displays their XRD patterns, and the lattice parameters were calculated and listed in Table 1. The XRD patterns of the exchanged products are similar to that of the precursor, which indicates that no significant structural change occurred during the ion exchange process. It can be seen from Table 1 that the lattice parameter *c* increased while *a* decreased after ion exchange reaction. The *d* spacings of the products washed with HCl aqueous solution become larger than that of δ-K_xMnO_2, which results in easy ion exchange. After the ion exchange reaction, there were more water molecules between the MnO_2 layers which stabilized the layer framework (shown in Table 3) leading to larger *d* spacings and larger lattice parameter *c*. The increase in the value of *c*/*a* indicates the characteristic of the layered structure.

Figure 2a shows the Fourier transform modulus F(*R*) spectra of the EXAFS at the Mn and Zr K-edges, while Fig. 2b displays the experimental (solid line) and fitting (dot line) EXAFS curves with k-weight of Mn–O and Zr–O coordination. The fitting parameters are listed in Table 2. The F(*R*) modulus of the EXAFS signal is a pseudo-radial distribution function around the absorber atoms. The different peaks can be associated to various neighbor shells and the positions of the peak maxima are linked to the bonding lengths (uncorrected from the backscattering phase shift at this stage). In the F(*R*) modulus at the Mn K-edge, the first peak located around 1.4 Å corresponds undoubtedly to the first oxygen neighbors; the second peak at about 2.2 Å corresponds to the second (transition metal) shell, which can be attributed to Mn-Mn second nearest neighbors. Curve-fitting analysis of the first shell of Mn revealed that the Mn-O bonding length in the material is 1.85 Å, close to that reported in literature (1.92 Å) [17–19]. Also, the coordination number is 5.2, which is lower than that of Mn in MnO_2 perfect crystal (6) due to the precision of *N* calculated by the EXAFS method estimated to be ≤20%. The Zr-O bonding length (2.12 Å) and coordination number (6.1) were obtained by the same method. J. Miehé-Brendlé et al. [20] reported the synthesis of Zr pillared beidellite by the intercalation method, and found that the simulation gives 6 O neighbors at 2.16 Å in pillared beidellite instead of 8 O neighbors at 2.22 Å of $ZrOCl_2$. The located structure of Zr in this work is similar to the results of the literature.

Figure 3 displays the schematic structure of pillared ZrO-MnO_2 from EXAFS results. Successive Mn layers

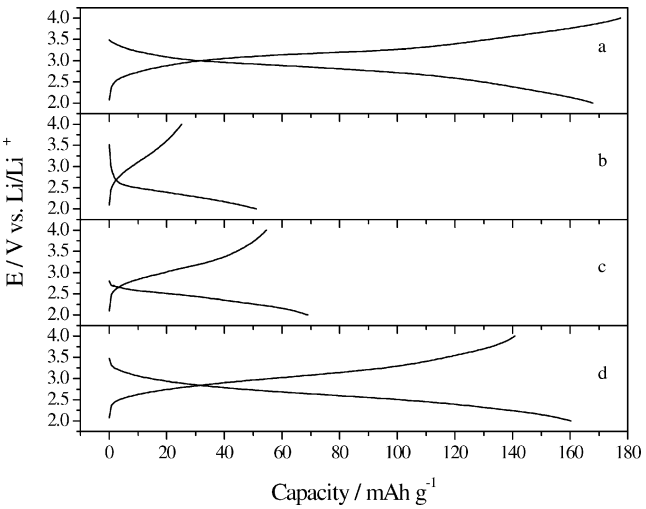

Fig. 4 Charge-discharge curves of the precursor and M-MnO_2 used as cathode materials. **a** Precursor K_xMnO_2. **b** Ba-MnO_2. **c** Sr-MnO_2. **d** ZrO-MnO_2

crystallized in hexagonal symmetry, and the negative charge resulted from Mn vacancy is compensated by ZrO^{2+} cations in octahedral coordination both above and below the MnO_2 sheets. Each Zr is coordinated to three O in the MnO_2 layer and three molecules of H_2O forming a H_2O sheet. Consequently, each Zr octahedron fills an octahedral site above the oxygen sheet and shares three corners with Mn octahedra, thus forming a tridentate corner-sharing octahedral interlayer complex.

Table 3 lists the chemical composition and the average oxidation state of Mn for the precursor and the exchange products. As shown in Table 3, most of the K^+ was extricated and Ba^{2+}, Sr^{2+} and ZrO^{2+} have been intercalated between the MnO_2 layers. The average oxidation state of Mn is close to that of the precursor, which indicates that the

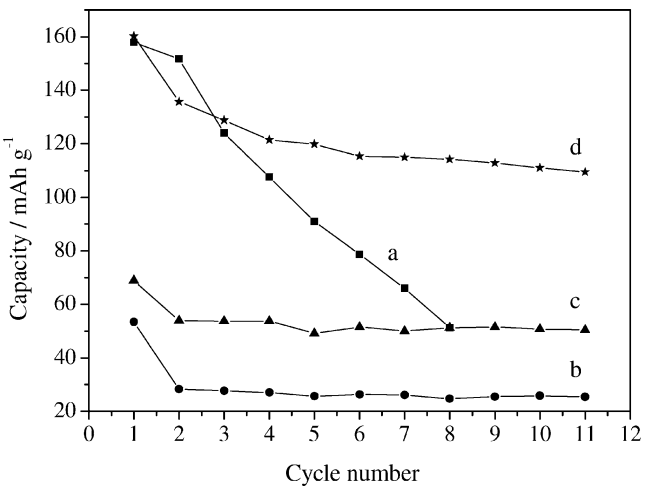

Fig. 5 Cycle performance of the cell with the precursor and M-MnO_2 as cathode materials. **a** Precursor K_xMnO_2. **b** Ba-MnO_2. **c** Sr-MnO_2. **d** ZrO-MnO_2

interlayer species are loosely bound and cation exchange can be readily carried out in birnessite.

Electrochemical performance of the samples

Composite electrodes were formed with the pillared materials and were dried at 120 °C in vacuum for 24 h to remove H_2O in the interlamellar space. Then cells were assembled and the discharge curves of the cell with the precursor and the three pillared compounds used as cathode materials are illustrated in Fig. 4. For the precursor which has an initial electromotive force (EMF) of 3.4 V and a capacity of 168.1 $mAh{\cdot}g^{-1}$ in the first discharge, the voltage decreases slowly over the whole discharge range from 4.0 to 2.0 V, indicative of single-phase behavior.

As shown in Fig. 4, the capacity decreased significantly as small amounts of Ba^{2+} or Sr^{2+} intercalated between MnO_2 layers compared with the precursor δ-K_xMnO_2. The capacity of the first discharge of Sr-MnO_2 and Ba-MnO_2 are 68.9 and 53.4 $mAh{\cdot}g^{-1}$, respectively, while the capacity of ZrO-MnO_2 reaches 161.5 $mAh{\cdot}g^{-1}$, close to that of the precursor. From the cycling profile it also can be seen that the discharge plateaus of the Sr-MnO_2 and Ba-MnO_2 are rather low, at about 2.3–2.4 V, indicating a remarkable electrode polarization. This is possibly related to the fact that diffusion of Li^+ ions in the materials was restricted because of the strong interaction between bivalent ions (Ba^{2+} and Sr^{2+}) and MnO_2 layers, which leads to a distinct polarization, and thus a potential drop and a lower capacity during discharge. While in the case of ZrO-MnO_2, the moderate interaction between pillars and layers results in fast diffusion of Li^+ ions and weak polarization, as a result a higher reversible capacity can be obtained.

Figure 5 displays the cycle performance of the precursor and M-MnO_2. In the subsequent cycles, the discharge capacity of K_xMnO_2 declined rapidly, and remains only 51 $mAh{\cdot}g^{-1}$ after the 8th cycling, about 32% of the first cycling. The cycling property of Ba-MnO_2 and Sr-MnO_2 materials are more stable after a small capacity drop in the first charge-discharge stage, and about 90–95% capacity maintains after the 10th cycling; whereas ZrO-MnO_2 has a relatively stable electrochemical property and the capacity remains at 110.0 $mAh{\cdot}g^{-1}$ after the 10th cycling.

Based on the results above, it can be concluded that the property of pillars has a significant influence on the structural stability and cycling behavior of layered MnO_2. When univalent ions K^+ locate in interlamellar space, weak interaction between the host matrix and the guest makes the structure unstable during cycling, resulting in a poor cycling property in spite of a large initial capacity. When divalent ions act as pillars, such as Ba-MnO_2 and Sr-MnO_2, although only a little capacity loss after many cycles was found due to the improved structural stability and enhanced cycling property, the strong interaction between layers and pillars leads to a low discharge capacity simultaneously. However, in the case of ZrO-MnO_2, the moderate interaction between layers and pillars results in a higher reversible capacity and relatively stable cycling behavior.

Conclusions

Pillared $M-MnO_2\left(M=Ba^{2+},Sr^{2+},ZrO^{2+}\right)$ were synthesized by the ion-exchange method, and their structure crystallized in the hexagonal system characterized by XRD, just as the precursor. In the material of ZrO-MnO_2, each Zr is coordinated to three O in MnO_2 and three molecules of H_2O forming a stable structure. The diffusion of Li^+ in the pillared materials $M-MnO_2$ $\left(M=Ba^{2+},Sr^{2+}\right)$ was restricted due to the strong interaction between pillars and the host matrix, which leads to an improved structural stability and enhanced cycling property albeit a reduced capacity. Among these materials, ZrO-MnO_2 has an advanced reversible capacity of 161.5 $mAh{\cdot}g^{-1}$ and improved cycling behavior compared with the precursor, which suggests ZrO-MnO_2 is a potential practical candidate as the cathode material for rechargeable lithium batteries.

Acknowledgements This project was supported by the National Natural Science Foundation Major International Joint Research Program (20620130108), National Natural Science Foundation of China (Grant No.: 20601001), the Program for New Century Excellent Talents in University (Project No.: NCET-05-121) and the III Project (Project No.: B07004).

References

1. Reed J, Ceder G, Van Der Ven A (2001) Electrochem Solid State Lett 4:A78
2. Paulsen JM, Mueller-Neuhaus JR, Dahn JR (2000) J Electrochem Soc 147:508
3. Armstrong AR, Bruce PG (1996) Nature 381:499
4. Armstrong AR, Gitzendanner R, Robertson AD, Bruce PG (1998) Chem Commun 1833
5. Paulsen JM, Dahn JR (1999) Solid State Ionics 126:3
6. Chen R, Zavalij P, Whittingham MS (1996) Chem Mater 8:1275
7. Zhang F, Ngala K, Whittingham MS (2000) Electrochem Commun 2:445
8. Chirayil TA, Zavalij PY, Whittingham MS (1996) J Electrochem Soc 143:L193
9. Zhang F, Zavalij PY, Whittingham MS (1997) Mater Res Bull 32:701
10. Zacalij PY, Zhang F, Whittingham MS (1997) Acta Cryst C 53:1738
11. Zacalij PY, Chirayil T, Whittingham MS, Pecharsky VK, Jacobson RA (1997) Acta Cryst C 53:170
12. Zhang F, Zavalij P, Whittingham MS (1999) Electrochem Commun 1:564

13. Zhang F, Whittingham MS (2000) Electrochem Commun 2:69
14. Liu P, Zhang J-G, Turner JA (2001) J Power Sources 92:204
15. Komaba S, Kumagai N, Chiba S (2000) Electrochim Acta 46:31
16. Delmas C, Fouassier Z (1976) Anorg Allg Chem 420:184
17. Drits VA, Silvester E, Gorshkov AI, Manceau A (1997) Am Mineral 82:942
18. Post JE, Appleman DE (1988) Am Mineral 73:1401
19. Manceau A, Lanson B, Drits VA (2002) Geochim Cosmochim Acta 66:2639
20. Miehé-Brendlé J, Khouchaf L, Baron J, Le Dred R, Tuilier M-H (1997) Micropor Mater 11:171